Phase composition and crystal structure of alumina-zirconia ceramics with varying $LaAl_{11}O_{18}$ content

Nina Cherkasova [a] *, Kristina Antropova [a], Aleksandr Legkodymov [bc], Igor Nasennik [ac], Georgiy Krivosheev [a], Urusveda Popova [a], Maria Zhulikova [a]

a: Novosibirsk State Technical University, Novosibirsk, 630073, Russia
b: Budker Institute of Nuclear Physics of the Siberian Branch of the RAS, Novosibirsk 630090, Russia
c: Synchrotron Radiation Facility SKIF, Boreskov Institute of Catalysis SB RAS, Kol'tsovo 630559, Russia
* Corresponding author: cherkasova.2013@corp.nstu.ru

Abstract

This study investigates the phase composition and structure of alumina-zirconia ceramics containing varying amounts of $LaAl_{11}O_{18}$ plates. The research addresses the significant influence of lanthanum hexaaluminate on the structural and physical properties of these ceramics, specifically focusing on its effects on crystal lattice parameters and phase volume content. Using synchrotron radiation and the Rietveld refinement method, the influence of lanthanum hexaaluminate content on the parameters of crystal lattices and phase content of the investigated materials were evaluated. Scanning electron microscopy was employed to analyze the grain size, morphology, and distribution within the material matrix. High-purity powders of α-Al_2O_3, 3Y-ZrO_2, and La_2O_3 were used as initial materials. The materials were obtained by the pressureless sintering techniques in two hours at 1520 °C. A series of materials comprising 50 wt.% ZrO_2 and varying percentage (0–15 wt.%) of $LaAl_{11}O_{18}$ was obtained. The coherent scattering regions of the alumina and zirconia matrix phases remained relatively unchanged in the composites. The coherent scattering regions of lanthanum hexaaluminate increased significantly with its concentration in the materials. The analysis revealed a decrease in alumina grain size with increasing $LaAl_{11}O_{18}$ content, while the size of the $LaAl_{11}O_{18}$ plates displayed a consistent increase. The best properties were observed for alumina-zirconia ceramics with the calculated content of lanthanum hexaaluminate of 12 wt.%. The relative density of this material is 95.3±0.3%, the hardness is 1490 Hv, and the indentation fracture resistance is 7.2±0.3 MPa·m$^{1/2}$.

Key findings

● $LaAl_{11}O_{18}$ content of 12 wt% is most effective in increasing fracture toughness.

● The grain sizes of alumina decrease with the increase in the lanthanum hexaaluminate content.

● The coherent scattering regions of lanthanum hexaaluminate increased significantly with its concentration in the materials.

1. Introduction

In recent years, there has been a steady growth of interest towards research into hexaaluminates of various chemical compositions [1–7]. This is largely due to the prospect of their application at high temperatures. Hexaaluminates are characterized by stable phase composition up to 1600 °C and resistance to thermal shocks [8]. Consequently, they are employed in the production of thermal barrier coatings [9]. In addition, the presence of hexaaluminates in the matrix of alumina-zirconia ceramics contributes to the growth of fracture toughness [10, 11]. This is due to the fact that the formation of plate structures of hexaaluminates slows and changes the direction of crack propagation in the material [12–15]. In paper [16], the authors studied Al_2O_3-$SrAl_{12}O_{19}$-3Y/4Y/5Y-ZrO_2 composite ceramics fabricated by the Pechini method. The material containing 8 vol% Al_2O_3 and 8 vol% $SrAl_{12}O_{19}$ in 3Y-ZrO_2 has the highest fracture toughness at 5.23±0.25 MPa·m$^{1/2}$, and the m-ZrO_2 content of 48.35±5.70% after low temperature degradation for 64 h.

In paper [17] Shi et al. studied the effect of CeO_2 on the structure and properties of Al_2O_3/Ti composites. The authors found that after the addition of CeO_2, the elongated phase $CeAl_{11}O_{18}$ was formed in the composites. The material with 2 mol.% CeO_2 is characterised by the highest bending strength and fracture toughness values of 576 MPa and 5.15 MPa·m$^{1/2}$, which increased by 21% and 20% compared to the Al_2O_3/Ti composite without CeO_2 addition. Ismail and Mohamad in [18] analysed the effect of $CaCO_3$ on the phase, physical, mechanical and microstructural properties of alumina-zirconia ceramics containing Nb_2O_5. The authors recorded the formation of elongated $CaAl_{12}O_{19}$ grains. At introduction of 1.0 wt.% $CaCO_3$ the highest values of fracture toughness were recorded, which are 5.84 MPa·m$^{1/2}$.

The synthesis characteristics of various hexaaluminate powders were also examined. In the study conducted by the authors of [19], the synthesis of $LaAl_{11}O_{18}$ and $BaAl_{12}O_{19}$ was explored utilizing various methods, including co-precipitation, wet impregnation, and solid-state synthesis, alongside distinct sintering profiles and a carbon templating approach. The impact of these different synthesis techniques and associated process parameters on the formation percentage of hexaaluminate phases was assessed, with phase identification corroborated through X-ray diffraction using Rietveld refinement and surface area determinations obtained via nitrogen physisorption. The co-precipitation method yielded $LaAl_{11}O_{18}$ with a commendable purity of 95%, as confirmed by Rietveld analysis of XRD data, resulting in a BET surface area of 2 m^2/g after sintering at 1600 °C. In contrast, the application of carbon templating effectively enhanced the surface area to 50 m^2/g when sintered at a reduced temperature of 1200 °C, albeit with a decrease in $LaAl_{11}O_{18}$ content to 77%. Notably, it was determined that $BaAl_{12}O_{19}$ could be synthesized at a lower temperature of 1400 °C, demonstrating a comparative advantage over $LaAl_{11}O_{18}$ synthesis conditions.

A special attention in a number of works was focused on lanthanum hexaaluminate ($LaAl_{11}O_{18}$, La-β-Al_2O_3), which has a defective magnetoplumbite structure. The crystal structure of lanthanum hexaaluminate is layered, consisting of blocks of aluminium oxide with spinel-like configuration, separated by monolayer mirror planes of symmetry, in which large La^{3+} cations are located [20, 21].

A number of papers reported different results on the effect of different lanthanum hexaaluminate content on the fracture toughness of alumina or alumina-zirconia ceramics.

Tang et al. in [22] studied the effect of $LaMgAl_{11}O_{19}$ content on the mechanical properties of Al_2O_3-$LaMgAl_{11}O_{19}$ composites obtained by pressureless sintering. It was found that $LaMgAl_{11}O_{19}$ addition has a positive effect on strength and fracture toughness at room temperature. The maximum value of 4.88 MPa·m$^{1/2}$ is observed at $LaMgAl_{11}O_{19}$ content of 9 wt.%, which is 13.4% higher than that of Al_2O_3 ceramics without additives (4.30 MPa·m$^{1/2}$).

In the article [23] the influence of La_2O_3 on the structure and properties of alumina-zirconia ceramics was evaluated. It was found that La_2O_3 can reduce the sintering temperature and increase the bending strength of the specimens. The bending strength and fracture toughness of composite ceramics with 1.5 wt.% La_2O_3 sintered at 1480 °C are 299.17 MPa and 5.61 MPa·m$^{1/2}$, respectively. Naga et al. in [24] studied Al_2O_3-$LaAl_{11}O_{18}$-ZrO_2 composites obtained by in situ sintering reaction of different ratios of Al_2O_3 and $La_2Zr_2O_7$. Only alumina, lanthanum hexaaluminate and zirconia were observed to form in the materials sintered in the temperature range of 1600 °C to 1725 °C within 1 h. Lanthanum zirconate and other intermediate phases were not detected. With increasing lanthanum hexaaluminate and zirconia content, the authors observed an increase in fracture toughness by more than three times compared to alumina ceramics.

Rivero-Antúnez et al. in [12] studied La-β-Al_2O_3/Al_2O_3 composites obtained by sol-gel synthesis. The fracture toughness of such materials is 6.5 MPa·m$^{1/2}$, which is 27% higher than that in the material without lanthanum hexaaluminate. The authors of this paper also focused considerable attention on the evolution of the crystal structure of the composites. X-ray diffraction data were studied by means of Rietveld refinements and line profile analyses; special attention was paid to the formation of lanthanum hexaaluminate, changes in the volume fraction and crystallite sizes of different phases at different temperatures.

At the same time, in most studies, insufficient attention is paid to the X-ray phase analysis of materials containing various hexaaluminates. It is of interest to evaluate the influence of the content of lanthanum hexaaluminate on the parameters of crystal lattice phases and the volume content of phases contained in the studied materials. For this purpose, in this research the obtained materials were investigated by synchrotron radiation, and the data were examined using the Rietveld method.

2. Materials and Methods

Submicron powders of α-Al_2O_3 (Almatis CT 3000 SG, D50 = 0.5 μm, 99.8 % purity), 3Y-ZrO_2 (Stanford Materials, D50 = 0.5 μm, 93.5 wt.% Zr(Hf)O_2; 5.5±0.2 wt.% Y_2O_3 purity) and La_2O_3 (D50 = 0.5 μm, 99.2% purity) were employed as the initial materials in this study. La_2O_3 powder was obtained by decomposition of lanthanum nitrate at 900 °C. The amount of zirconia in all investigated compositions was 50 wt.%, lanthana was introduced in the amount from 0.43 to 3.37 wt.%, and the rest was alumina. The content of lanthana was calculated to form 0 to 15 wt.% $LaAl_{11}O_{18}$ in the sintered materials. The selection of the zirconia content in this study is based on our previous research findings. Specifically, alumina-zirconia ceramics, composed of equal proportions of each component and synthesized through pressureless sintering, exhibited

optimal bending strength alongside enhanced fracture toughness and hardness [25].

Aqueous suspensions (50% solid content) were prepared, with 2 wt.% of Dolapix deflocculant added to enhance deagglomeration of the powders. Prior to granulation, 1 wt.% of a 10 wt.% polyvinyl alcohol (PVA) solution (grade 16/1) and 1 wt.% of polyethylene glycol (PEG 400) powder were incorporated into the mixtures.

The suspensions were dispersed in a ball mill for 24 h, utilizing zirconia grinding bodies with a diameter of 0.8 mm. Following the evaporation of water from the suspensions, the resulting dry mass was ground in a ceramic mortar with a ceramic pestle and subsequently sieved through mesh sizes ranging from 100 to 250 μm. Beam-shaped specimens were produced by uniaxial pressing of the granulated powders at a pressure of 100 MPa using an Instron 3369 testing machine. Sintering was conducted in a tube furnace at a temperature of 1520 °C for 2 h under atmospheric conditions.

The investigation of the formed phases included the determination of lattice parameters through X-ray diffraction analysis. The diffraction patterns were obtained at the Siberian Centre for Synchrotron and Terahertz Radiation at the VEPP-4 electron accelerator (Novosibirsk, Institute of Nuclear Physics SB RAS, channel 8-A, hard X-ray diffraction). The synchrotron X-ray radiation served as a photon source. The diffraction patterns were recorded in the 'lumen' mode utilizing a Mar354s two-axis detector with a pixel size of 100×100 μm² and a scanning diameter of 345 mm. Monochromatic radiation was generated using a silicon butterfly-type crystal, resulting a beam size of 200×200 μm, with a wavelength of 0.178 Å.

The ring diffraction patterns were averaged via azimuthal integration using the PyFAI (Python Fast Azimuthal Integration) package. Initially, the diffraction profiles were refined using a pseudo-Voit function combined with a fifth-degree polynomial to estimate the background, facilitating the determination of the lattice parameters. Profile analysis enabled the identification of the positions of the X-ray maxima corresponding to the desired phases. Subsequently, based on the Wolf-Bragg equation, a system of equations specific to the given phase was formulated and solved using the least squares method.

$$\begin{cases} 2d_0 \sin\theta_0 = \lambda \\ 2d_1 \sin\theta_1 = \lambda \\ \quad\quad ... \\ 2d_n \sin\theta_n = \lambda \end{cases}, \quad (1)$$

where d_i – interplanar spacing; θ_i – angle corresponding to the interplanar spacing d_i; λ – wavelenght; n – number of analyzed reflections of the studied phase.

Mathematical criterion of diffraction profiles approximation quality was evaluated using R-factor according to the formula:

$$R = \sum_i \frac{|I_e - I_c|}{I_c}, \quad (2)$$

where I_e – experimental intensity values and I_c – values obtained by calculation.

The phases were identified using the ICDD PDF 4+ database. Profex 5.2.0 programme was used to process the diffraction patterns by the Rietveld refinement method [26].

The apparent density and open porosity were determined for the sintered specimens by hydrostatic weighing. The AD-1653 density determination complex established on AND GR-300 analytical scale was used. The theoretical density of the composites was calculated. The relative density of the sintered materials under study was estimated.

Structural investigations of the specimens were performed using a Carl Zeiss EVO 50 scanning electron microscope at magnifications up to x20000. Preliminarily, slides were prepared according to standard technology using diamond suspensions.

The specimens were etched with concentrated hydrofluoric acid for 10 seconds. The obtained images were processed and analyzed using the JMicroVision software version 1.2.7 [27]. At least 200 grains of each chemical composition were measured to estimate grain size.

Vickers hardness and indentation fracture resistance (K_{IFR}) was determined by the indentation method [28]. The tests were performed using an EMCO-TEST DuraScan 50 testing machine. A diamond Vickers pyramid was used as the indenter. The load was 10 kg. At least 5 indents were obtained on each specimen.

After the measurements, the values of the K_{IFR} were calculated according to formula Niihara formula, in which the contribution of the Young's modulus of materials is included [29]:

$$K_{Ic} = 0.048 \cdot \left(\frac{c}{a}\right)^{-0.5} \cdot \left(\frac{H_v}{E\varphi}\right)^{-0.4} \cdot \frac{H_v \cdot a^{0.5}}{\varphi}, \text{MPa} \cdot m^{1/2} \quad (3)$$

where K_{IC} is the fracture toughness, H_V – hardness, GPa; E – Young's modulus, GPa; c –crack length, μm; a – half-diagonal length of an indentation, μm; φ – constraint factor ($\varphi = 3$).

3. Results and Discussion

The changes in apparent density and apparent porosity of the investigated materials were evaluated by varying the lanthana content in the initial mixtures (Table 1). The relative density of alumina ceramics without additives was measured at 95.5±0.3%. The introduction of the minimal lanthana amounts into the composites resulted in a decrease in relative density compared to the initial material without additives. The lowest relative density value was 90.5% for the samples with 9 wt.% $LaAl_{11}O_{18}$ in the sintered material [30]. However, the materials containing calculated concentrations of lanthanum hexaaluminate at 12 and 15 wt.% exhibited relative densities of 95.3±0.3% and 95.6±0.3%, respectively.

Table 1 Relative density and open porosity of the investigated materials.

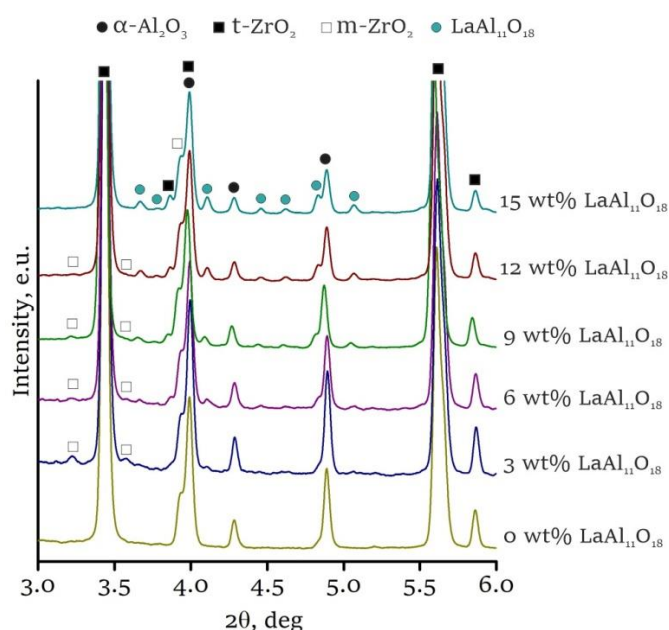| Calculated content of LaAl$_{11}$O$_{18}$, wt.%	Relative density, %	Open porosity, %
0	95.5±0.3	1.2±0.2
3	93.5±0.2	2.3±0.1
6	92.0±0.3	2.5±0.2
9	90.5±0.5	2.7±0.3
12	95.3±0.3	2.2±0.3
15	95.6±0.3	2.3±0.3

This indicates that the presence of hexaaluminate promotes the formation of denser and more homogeneous ceramics within the Al$_2$O$_3$-ZrO$_2$ system. Similar phenomena were documented in the literature on similar topics. It is known that cations of hexaaluminate-forming additives can distribute along the boundaries of alumina grains, inhibiting grain growth and, consequently, enhancing densification during the sintering process [31, 32]. Furthermore, the asymmetric morphology of the formed hexaaluminate plates significantly contributed to the observed decrease in density and porosity [22, 33, 34]. This plate shape promotes the development of microcracks and pores, which, in turn, alters the physical properties of the investigated materials.

In this study, X-ray phase analysis was employed to identify the phases present in the materials (Figure 1). The analysis revealed that the primary phases were α-Al$_2$O$_3$ and t-ZrO$_2$, confirming their significant presence in the material structure. In addition, X-ray reflections corresponding to the LaAl$_{11}$O$_{18}$ compound were detected during the analysis. The introduction of lanthana into the matrix facilitated the formation of lanthanum hexaaluminate across all compositions examined.

Moreover, the presence of m-ZrO$_2$ were identified in several materials, likely linked to increases in specimens porosity, which may induce the phase transition from tetragonal to monoclinic transformation in the 3Y-ZrO$_2$ system. This transformation is attributed to the lack of compressive stresses on the matrix grains, allowing them to undergo free transformation in their crystal structure. Similar effects were reported in the previous research involving materials with calcium hexaaluminate [35]. The research [36] also recorded the appearance of m-ZrO$_2$ in materials containing LaAl$_{11}$O$_{18}$. The authors attributed this effect to the lower hardness and modulus of elasticity of LaAl$_{11}$O$_{18}$, which also led to a decrease in compressive stresses on ZrO$_2$ and its t-m phase transformation.

Rietveld analysis was conducted on the X-ray diffraction (XRD) data, allowing us to extract both qualitative and quantitative information regarding the material phases present. Specifically, we calculated the mass content of each phase, the coherent scattering regions, and the crystal lattice parameters. The results of the phase composition calculations, as determined by the Rietveld method, are summarized in Table 2. Overall, the measured phase content values are in close agreement with the expected values. Notably, minor deviations observed in the LaAl$_{11}$O$_{18}$ content can be attributed to measurement error. Furthermore, the presence of monoclinic zirconia (m-ZrO$_2$) in quantities not exceeding 1 wt.% does not adversely affect the mechanical properties of the materials.

The lattice parameters of the primary phases present in the investigated materials are presented in Table 3. The data analysis reveals that the lattice parameters of tetragonal zirconia (t-ZrO$_2$) exhibit non-linear variations. The degree of tetragonality for all studied materials ranges from 1.433 to 1.435, indicating structural stability. The lack of significant changes in the degree of tetragonality suggests that La^{3+} cations do not dissolve into the crystal lattice of t-ZrO$_2$ stabilized by 3 mol.% Y$_2$O$_3$. Additionally, it was observed that the c parameter for the LaAl$_{11}$O$_{18}$ compound increases with an increase in its content within the material, while the a:c ratio shows a decreasing trend.

Figure 1 X-ray phase analysis of investigated materials.

Table 2 Phase content experimentally determined by the Rietveld method, wt.%.

Calculated content of LaAl$_{11}$O$_{18}$, wt. %	α-Al$_2$O$_3$	t-ZrO$_2$	m-ZrO$_2$	LaAl$_{11}$O$_{18}$	GOF
0	49.7±0.8	50.3±0.8	–	–	1.105
3	48.1±0.6	48.1±0.5	1.1±0.4	3.7±0.7	1.115
6	43.1±0.2	49.6±0.2	1.1±0.3	6.2±0.2	1.254
9	41.2±0.6	49.2±0.5	0.8±0.2	8.8±0.5	1.285
12	37.4±0.1	50.3±0.8	0.5±0.2	11.8±0.1	1.121
15	33.7±0.1	52.3±0.9	–	14.0±0.8	1.262

Table 3 Crystal lattice parameters of the investigated materials.

Calculated content of $LaAl_{11}O_{18}$, wt.%	α-Al_2O_3	t-ZrO_2	$LaAl_{11}O_{18}$	$LaAl_{11}O_{18}$ aspect ratio a:c
0	a = b = 4.728 c = 13.003	a = b = 3.618 c = 5.189	-	-
3	a = b = 4.730 c = 13.005	a = b = 3.616 c = 5.183	a = b = 5.589 c = 21.558	0.2593
6	a = b = 4.723 c = 13.003	a = b = 3.631 c = 5.202	a = b = 5.567 c = 21.870	0.2545
9	a = b = 4.727 c = 13.006	a = b = 3.626 c = 5.210	a = b = 5.579 c = 21.961	0.2540
12	a = b = 4.722 c = 12.999	a = b = 3.615 c = 5.188	a = b = 5.558 c = 21.950	0.2532
15	a = b = 4.689 c = 12.975	a = b = 3.618 c = 5.190	a = b = 5.554 c = 22.010	0.2523

These changes may indicate interactions between phases in the studied system and warrant further detailed analyses to elucidate their impact on the properties and structure of the materials.

Coherent scattering regions (SCRs) were also measured. For t-ZrO_2 and α-Al_2O_3, the SCRs remain unchanged at 22.94 and 22.93 nm, respectively. In contrast, for the $LaAl_{11}O_{18}$, the SCRs increase with the content of this phase in the material, ranging from 26 nm to 80 nm. Furthermore, the microstresses associated with $LaAl_{11}O_{18}$ increase as its content rises from 0.00153 to 0.00373.

In the course of the structural investigations of the Al_2O_3-ZrO_2-$LaAl_{11}O_{18}$ composite system, the presence of characteristic plate-like grains was identified. By EDX analysis, it was found that the plate is composed of La, Al and O elements (Figure 3). Thus it is confirmed that the plate is $LaAl_{11}O_{18}$. The results presented in Figure 2 were obtained using a scanning electron microscope (SEM) operating in the secondary electron emission mode. A predominantly uniform distribution of grains was observed in the structure of the materials investigated; however, localized clusters of grains belonging to a single phase were also identified. Notably, in the specimen exhibiting the highest concentration of $LaAl_{11}O_{18}$, distinct clusters of plate-like grains were present. This phenomenon may be attributed to the dispersion mechanisms inherent to the material processing methods employed. Table 4 provides a summary of the grain sizes of materials analyzed. Notably, the length of the lanthanum hexaaluminate plates exhibited an increase, ranging from 1.12 to 1.49 μm, as the content of $LaAl_{11}O_{18}$ in the composites elevated from 3 to 15 wt.%. The width of the plates remained consistent at 0.2 μm for all compositions containing $LaAl_{11}O_{18}$ up to 12 wt.%. In contrast, a material composition with 15 wt.% $LaAl_{11}O_{18}$ revealed an increase in plate width to 0.3 μm. Throughout all compositions examined, the aspect ratio of the plates was consistently 6:1. Furthermore, the observed increase in the dimensions of the lanthanum hexaaluminate plates correlates positively with the rise in specific conductivity values (SCRs) as the $LaAl_{11}O_{18}$ content in the material increases.

The influence of additive content on the grain size of alumina was systematically evaluated. It was observed that the addition of lanthanum hexaaluminate plates results in a decrease in alumina grain size, attributed to the interaction with the lanthanum-containing additive. At an additive concentration of 12 wt.%, the alumina grain size measures 0.65 μm. This reduction can be explained by the propensity of lanthanum to segregate along the boundaries of the alumina grains, effectively hindering their migration and growth [37]. This phenomenon is consistent with findings reported in several studies [31, 38].

However, in the composite containing 15 wt.% $LaAl_{11}O_{18}$, the size of the alumina grains increases to 0.75 μm. At the same time, a significant decrease in the volume fraction of alumina is observed. We hypothesize that this reduction is likely due to a considerable fraction of the alumina grains being consumed during the synthesis of lanthanum hexaaluminate. Interestingly, the sizes of zirconia grains remain unchanged, which is consistent with the measurements of crystal lattice parameters and coherent scattering regions of t-ZrO_2. The stability of these structural parameters under the influence of oxide additives and the formation of new phases suggests a robust structural integrity of the zirconia component in the composites.

The hardness and indentation fracture resistance (K_{IFR}) of the investigated materials were evaluated. The results are presented in Table 5. It was observed that the hardness of materials decreases with increasing content of lanthanum hexaaluminate. These findings correlate with our previous research on hexaaluminates of different chemical composition [35, 39] and agree with the results reported by other research groups [40]. The observed decrease in hardness is attributed to the reduced content of the hardest phase, alumina, within the composite materials.
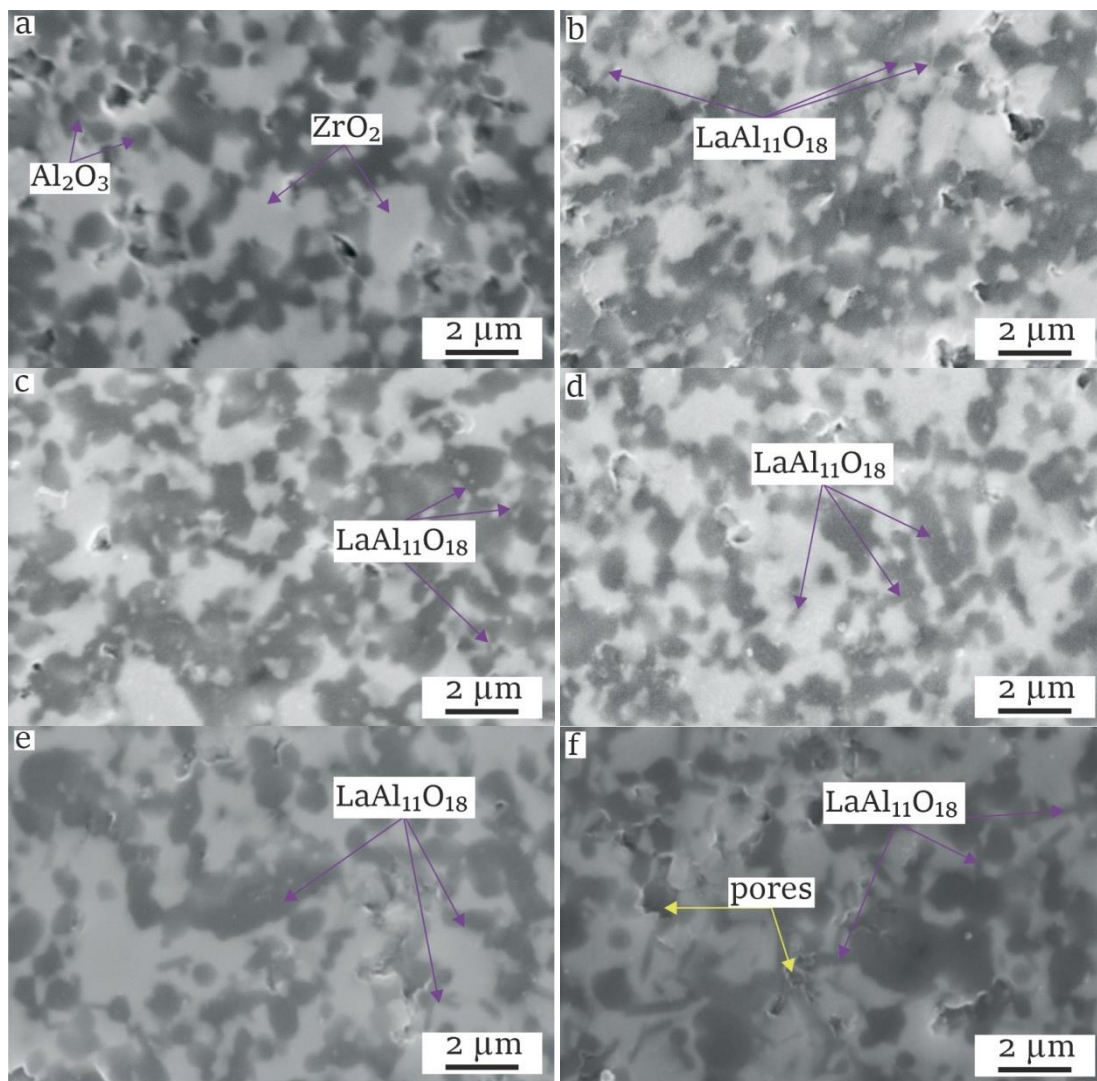
Figure 2 Structure of the investigated materials: alumina-zirconia ceramics without additives (a); with 3 wt.% $LaAl_{11}O_{18}$ (b), with 6 wt.% $LaAl_{11}O_{18}$ (c), with 9 wt.% $LaAl_{11}O_{18}$ (d), with 12 wt.% $LaAl_{11}O_{18}$ (e), with 15 wt.% $LaAl_{11}O_{18}$ (f).

Table 4 Grain sizes of investigated materials.

Chemical composition	Al_2O_3 average grain size (µm)	The size of the $LaAl_{11}O_{18}$ plates		
		Length (µm)	Width (µm)	Aspect ratio
Without $LaAl_{11}O_{18}$	0.78±0.13	–	–	–
3 wt.% $LaAl_{11}O_{18}$	0.67±0.08	1.12±0.07	0.20±0.01	6
6 wt.% $LaAl_{11}O_{18}$	0.65±0.07	1.12±0.06	0.20±0.01	6
9 wt.% $LaAl_{11}O_{18}$	0.65±0.06	1.13±0.05	0.21±0.01	6
12 wt.% $LaAl_{11}O_{18}$	0.65±0.07	1.40±0.07	0.22±0.01	7
15 wt.% $LaAl_{11}O_{18}$	0.75±0.04	1.49±0.08	0.26±0.02	6
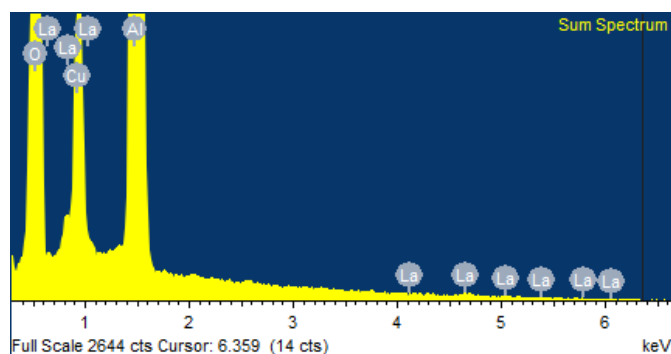
Figure 3 EDX analysis of the $LaAl_{11}O_{18}$ plate.

The K_{IFR} of all materials containing $LaAl_{11}O_{18}$ is higher than that of the material without additive. However, the K_{IFR} indices of the investigated materials exhibit an uneven variation with increasing lanthanum hexaaluminate content. The lowest values of K_{IFR} were recorded for the material with 9 wt.% $LaAl_{11}O_{18}$, which also displayed the lowest density and a high porosity level. It is likely that the substantial presence of pores adversely affected the critical stress intensity factor in this material. In contrast, the most significant increase in indentation fracture resistance – by 45% compared to alumina-zirconia ceramics without additives – was observed in the material containing 12 wt.% $LaAl_{11}O_{18}$.

Table 5 Hardness and indentation fracture resistance of the investigated materials.

Calculated content of LaAl$_{11}$O$_{18}$, wt.%	Hardness, Hv$_{0,5}$	K_{IFR}, MPa·m$^{1/2}$
0	1650±70	5.0±0.2
3	1600±60	6.2±0.3
6	1550±60	6.0±0.2
9	1490±35	5.5±0.1
12	1490±40	7.2±0.3
15	1480±40	6.5±0.2

This particular sample exhibited an aspect ratio of 7, whereas the other materials had an aspect ratio of 6. This difference in aspect ratios is likely a contributing factor to the enhanced K_{IFR}. The substantial effect of aspect ratios on toughness was previously discussed in [17], who noted that the role of CeAl$_{11}$O$_{18}$ in strengthening Al$_2$O$_3$/Ti composites was directly related to the aspect ratio of the elongated particles, which in turn was associated with the CeO$_2$ content.

The observed decrease in the K_{IFR} with increasing lanthanum hexaaluminate content is attributed to several factors: an increase in porosity and a reduction in material density. The observed changes in the character of the K_{IFR} are likely influenced by variations in alumina grain size. A decrease in alumina grain size is associated with an increase in the K_{IFR}. However, it is essential to note that these changes are non-linear, as porosity also significantly contributes to the mechanical properties of the materials. The increase in alumina grain size in the material with maximum LaAl$_{11}$O$_{18}$ content probably also affected the decrease in K_{IFR}. Similar results were reported in various studies.

To further investigate the mechanisms underlying the observed increase in indentation fracture resistance, a detailed analysis of crack propagation trajectories was conducted (Figure 4). Different mechanisms of indentation fracture resistance enhancement were identified. For example, plate fracture is observed, as well as crack stopping on plate impact, as indicated by the ovals in the figure. Crack envelopment around Al$_2$O$_3$-grains is also encountered. In [41], the authors investigated Al$_2$O$_3$-ZrO$_2$ ceramics containing LaAl$_{11}$O$_{18}$ plates, which were obtained via vat photopolymerization based 3D printing techniques. Through a combination of theoretical modeling and experimental observations, the authors concluded that the high elastic modulus of the matrix generates substantial compressive stresses on the elongated LaAl$_{11}$O$_{18}$ grains, making them resistant to pull-out. Consequently, LaAl$_{11}$O$_{18}$ grains experience significant compressive stresses, influencing crack propagation to preferentially traverse through these grains. This behavior promotes transgranular fracture and, as the crack interacts with the LaAl$_{11}$O$_{18}$ plates, it dissipates a considerable amount of energy, leading to crack arrest, which frequently occurs within the LaAl$_{11}$O$_{18}$ plates themselves.
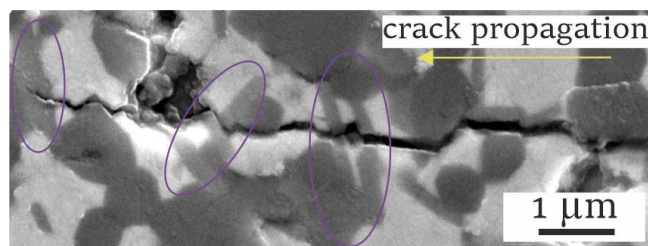
Figure 4 Crack propagation in the material with 12 wt.% LaAl$_{11}$O$_{18}$.

4. Limitations

In this research, alumina-zirconia ceramics were obtained using pressureless sintering technology. This method resulted in materials with relatively high porosity, which influences the mechanical properties, specifically, hardness and fracture toughness. To improve the quality of the ceramics, it is recommended to explore load-assisted sintering techniques, such as spark plasma sintering or hot pressing. These alternative methods have the potential to produce materials with minimal porosity and densities closer to their theoretical values, thereby mitigating the impact of porosity on the mechanical properties of the ceramics. Localized clusters of single-phase grains were observed during the investigation, potentially linked to the dispersion methods employed in the study. To achieve a more uniform distribution of phases within the material, it may be advantageous to utilize a high-energy bead mill for dispersion instead of a ball rolling mill.

5. Conclusions

In all investigated materials, lanthanum hexaaluminate was formed when lanthana was introduced. The coherent scattering regions of matrix phases of α-Al$_2$O$_3$ and t-ZrO$_2$ practically do not change in the investigated composites, and the SCRs of lanthanum hexaaluminate significantly increases with the increase of its content in the materials. The Al$_2$O$_3$-grain sizes decrease with the increase in the lanthanum hexaaluminate content, and the size of plates, on the contrary, increases.

The best properties were observed for alumina-zirconia ceramics with calculated content of lanthanum hexaaluminate 12 wt.%. The material of this composition exhibits a highly rational combination of several key characteristics: a substantial content of LaAl$_{11}$O$_{18}$ plates, a high aspect ratio of these plates, the smallest Al$_2$O$_3$-grain size measured at 0.65 μm, and a superior relative density compared to the other compositions studied. According to the data of X-ray phase analysis and Rietveld calculations, such material contains 37.4±0.1 wt.% Al$_2$O$_3$, 50.3±0.8 wt.% t-ZrO$_2$, 0.5±0.2 wt.% m-ZrO$_2$ and 11.8±0.1 wt.% LaAl$_{11}$O$_{18}$. The obtained values are close to the calculated values. The relative density of this material is 95.3±0.3 wt.%, the hardness is 1490 Hv, and the indentation fracture resistance is 7.2±0.3 MPa·m$^{1/2}$.

Supplementary materials

Acknowledgments

Author contributions

Conceptualization: N.Ch., K.A.
Data curation: I.N.
Formal Analysis: N.Ch., K.A., I.N.
Investigation: N.Ch., K.A., A.L., I.N, M.Zh.
Methodology: K.A., A.L., G.K., U.P.
Validation: N.Ch., K.A.
Visualization: G.K., U.P., M.Zh.
Writing – original draft: N.Ch., K.A.

Conflict of interest

The authors declare no conflict of interest.

Additional information

Author IDs:

Nina Cherkasova, Scopus ID 56971176200;
Kristina Antropova, Scopus ID 57759105600;
Aleksandr Legkodymov, Scopus ID 8957964700.

Website:

Novosibirsk State Technical University, https://www.nstu.ru/.

References

1. Yin X, Zhang B, Wang H, Li X, Feng Q. Enhancement of sintering and mechanical properties of alumina-rich Al_2O_3-MgO-CaO refractory composite by doping La_2O_3. Ceram Int. 2024;50(22):47494–500. doi:10.1016/j.ceramint.2024.08.492

2. Suzuki Y, Nishihashi K. Microstructures and mechanical properties of reactively sintered $CaAl_{12}O_{19}/CaAl_4O_7$ porous composites. Ceram Int. 2023;49(18):29427–32. doi:10.1016/j.ceramint.2023.06.004

3. Jin Y, Wang S, Zhang Y, Gao H, Zhou X, Li D, Yang H, Fang L, Jagadeesha AV, Ubaidullah M, Pandit B, Zhang H. Rare earth ions (Er, Ho and Sm) regulate the optical and photoluminescence properties of $CaAl_{12}O_{19}$: Performance prediction and anti-counterfeiting application. Ceram Int. 2024;50(9):16096–110. doi:10.1016/j.ceramint.2024.02.090

4. Kern F, Gadow R. In Situ Platelet Reinforcement of Alumina and Zirconia Matrix Nanocomposites – One Concept, Different Reinforcement Mechanisms. Adv Sci Technol. 2014;87:118–25. doi:10.4028/www.scientific.net/AST.87.118

5. Podzorova LI, Shvorneva LI, Il'Icheva AA, Alad'Ev NA, Pen'Kova OI. Microstructure and phase composition of ZrO_2-CeO_2-Al_2O_3 materials modified with MgO and Y_2O_3. Inorg Mater. 2013;49(4):376–81. doi:10.1134/S0020168513030163

6. Bugaeva AY, Nazarova LY, Belyi VA, Ryabkov YI. Phase Transformations of Zirconium Dioxide and Crystal Growth During Heat Treatment of the $ZrO_2(CeO_2,Y_2O_3)$–$La_{0.85}Y_{0.15}Al_{11}O_{18}$–$Al_2O_3$ System. Russ J Gen Chem. 2022;92(8):1488–97. doi:10.1134/S1070363222080175

7. Podzorova LI, Kutuzova VE, Il'ichyova AA, Pen'kova OI, Sirotinkin VP, Konovalov AA, Antonova OS, Baikin AS. Composites of the Al_2O_3/Yb-TZP System Modified with Calcium, Strontium, and Barium Cations. Inorg Mater Appl Res. 2022;13(5):1318–23. doi:10.1134/S2075113322050343

8. Wu C, Zhan L, Liu Q, Liu H, Wang J, Liu W, Yao S, Ma Y. Grain boundary segregation for enhancing the thermal stability of alumina-mullite diphasic fibers by La_2O_3 addition. J Eur Ceram Soc. 2023;43(15):7012–22. doi:10.1016/j.jeurceramsoc.2023.07.017

9. Chen X, Sun Y, Chen D, Li J, Li W, Zeng D, Wu D, Zou B, Cao X. A comparative investigation on the corrosion degradation of plasma sprayed YSZ and $LnMgAl_{11}O_{19}$ (Ln = Nd, Sm, Gd) coatings exposed to the molten V_2O_5 + Na_2SO_4 salt mixture at 1100 ºC. J Eur Ceram Soc. 2019;39(13):3778–87. doi:10.1016/j.jeurceramsoc.2019.04.055

10. Sarath Chandra K, Monalisa M, Chowdary CVA, Ghosh G, Sarkar D. Microstructure and mechanical behaviour of SrO doped Al_2O_3 ceramics. Mater Sci Eng A. 2019;739:186–92. doi:10.1016/j.msea.2018.10.038

11. Kern F, Gommeringer A. Reinforcement Mechanisms in Yttria-Ceria-Co-Stabilized Zirconia- Alumina-Strontium Hexaaluminate Composite Ceramics 2018;98:93–8. doi:10.4416/JCST2017-00046

12. Rivero-Antúnez P, Morales-Flórez V, Cumbrera FL, Esquivias L. Rietveld analysis and mechanical properties of in situ formed La-β-Al_2O_3/Al_2O_3 composites prepared by sol-gel method. Ceram Int. 2022;48(17):24462–70. doi:10.1016/j.ceramint.2022.05.058

13. Zhang F, Chevalier J, Olagnon C, Meerbeek B Van, Vleugels J. Slow crack growth and hydrothermal aging stability of an alumina-toughened zirconia composite made from La_2O_3-doped 2Y-TZP. J Eur Ceram Soc. 2017;37(4):1865–71. doi:10.1016/J.JEURCERAMSOC.2016.11.003

14. Guo R, Guo D, Chen Y, Yang Z, Yuan Q. In situ formation of LaAl11O18 rodlike particles in ZTA ceramics and effect on the mechanical properties. Ceram Int. 2002;28(7):699–704. doi:10.1016/S0272-8842(02)00031-7

15. Sktani ZDI, Rejab NA, Ahmad ZA. Tougher and harder zirconia toughened alumina (ZTA) composites through in situ microstructural formation of $LaMgAl_{11}O_{19}$. Int J Refract Met Hard Mater. 2019;79:60–8. doi:10.1016/J.IJRMHM.2018.11.009

16. Li Q, Chen K, Ng T, Yang Y, Luo H, Zhang C, Huang Y, Jian Y, Zhao K, Wang X. Development and characterization of Al_2O_3/$SrAl_{12}O_{19}$ reinforced zirconia with high fracture toughness and low-temperature degradation-resistant for dental applications. J Mater Res Technol. 2024;30:6877–88. doi:10.1016/j.jmrt.2024.05.051

17. Shi S, Cho S, Goto T, Sekino T. Role of $CeAl_{11}O_{18}$ in reinforcing Al_2O_3 /Ti composites by adding CeO_2. Int J Appl Ceram Technol. 2021;18(1):170–81. doi:10.1111/ijac.13629

18. Ismail H, Mohamad H. Effects of $CaCO_3$ additive on the phase, physical, mechanical, and microstructural properties of zirconia-toughened alumina-CeO_2-Nb_2O_5 ceramics. Ceram Int. 2023. doi:10.1016/j.ceramint.2023.09.015

19. Seyidoglu T. Investigation and production of high purity lanthanum and barium hexaaluminate ceramic powders. Open Ceram. 2023;16:100491. doi:10.1016/j.oceram.2023.100491.

20. Heveling J. La-Doped Alumina, Lanthanum Aluminate, Lanthanum Hexaaluminate, and Related Compounds: A Review Covering Synthesis, Structure, and Practical Importance. Ind Eng Chem Res. 2023;62(6):2353–86. doi:10.1021/acs.iecr.2c03007

21. Torrez-Herrera JJ, Korili SA, Gil A. Progress in the synthesis and applications of hexaaluminate-based catalysts. Catal Rev. 2022;64(3):592–630. doi:10.1080/01614940.2020.1831756

22. Tang H, Fang M, Tang C, Huang Z, Liu H, Zhu H, Liu Y, Wu X. Effect of $LaMgAl_{11}O_{19}$ addition and temperature on the mechanical properties of Al_2O_3-based ceramics. Mater Sci Eng A. 2016;655:160–7. doi:10.1016/J.MSEA.2015.12.097

23. Xu X, Xie G, Wu J, Wei P, Chen Z, Ma S. Preparation and thermal shock resistance investigation of ZTA-La_2O_3 composite ceramics for porous medium combustion materials. Ceram Int. 2023;49(11):18645–53. doi:10.1016/j.ceramint.2023.02.241

24. Naga SM, Hassan AM, El-Maghraby HF, Awaad M, Elsayed H. In-situ sintering reaction of Al_2O_3–LaAl11O18–ZrO2 composite. Int J Refract Met Hard Mater. 2016;54:230–6.

doi:10.1016/j.ijrmhm.2015.07.026

25. Cherkasova N, Veselov S, Bataev A, Kuzmin R, Stukacheva N. Structure and mechanical properties of ceramic materials based on alumina and zirconia with strontium hexaaluminate additives. Mater Chem Phys. 2021;259:123938. doi:10.1016/j.matchemphys.2020.123938

26. Doebelin N, Kleeberg R. Profex : a graphical user interface for the Rietveld refinement program BGMN. J Appl Crystallogr. 2015;48(5):1573–80. doi:10.1107/S1600576715014685

27. N. Roduit, JMicroVision: Image analysis toolbox for measuring and quantifying components of high-definition images. Version 1.3.4, Software available for free download at https://jmicrovision.github.io/.

28. Sktani ZDI, Rejab NA, Ratnam MM, Ahmad ZA. Fabrication of tougher ZTA ceramics with sustainable high hardness through (RSM) optimisation. Int J Refract Met Hard Mater. 2018;74:78–86. doi:10.1016/j.ijrmhm.2018.03.006

29. Niihara K, Morena R, Hasselman DPH. Evaluation of K Ic of brittle solids by the indentation method with low crack-to-indent ratios. J Mater Sci Lett. 1982;1(1):13–6. doi:10.1007/BF00724706

30. Cherkasova NY, Antropova KA, Kuchumova ID, Fedorenko EA, Kim EY, Kiseleva IY. Preparation and Research of Composite Materials of the Al_2O_3–ZrO_2–La_2O_3 System. Refract Ind Ceram. 2023;64(1):63–6. doi:10.1007/s11148-023-00805-1

31. Rani DA, Yoshizawa Y, Hirao K, Yamauchi Y. Effect of Rare-Earth Dopants on Mechanical Properties of Alumina. J Am Ceram Soc. 2004;87(2):289–92. doi:10.1111/j.1551-2916.2004.00289.x

32. Gülgün MA, Voytovych R, Maclaren I, Rühle M, Cannon RM. Cation segregation in an oxide ceramic with low solubility: Yttrium doped α-alumina. Interface Sci. 2002;10(1):99–110. doi:10.1023/A:1015268232315

33. Naga SM, Elshaer M, Awaad M, Amer AA. Strontium hexaaluminate/ZTA composites: Preparation and characterization. Mater Chem Phys. 2019;232:23–7. doi:10.1016/j.matchemphys.2019.04.055

34. Negahdari Z, Willert-Porada M, Pfeiffer C. Mechanical properties of dense to porous alumina/lanthanum hexaaluminate composite ceramics. Mater Sci Eng A. 2010;527(12):3005–9. doi:10.1016/j.msea.2010.01.050

35. Cherkasova N, Antropova K, Kuzmin R, Emurlaev K, Kuchumova I, Burkhinova N, Zobova Y. Features of calcium hexaaluminate formation in alumina-zirconia ceramics. Chim Techno Acta. 2023;10(3). doi:10.15826/chimtech.2023.10.3.17

36. Aziz HS, Wan C, Xing Y, Sajid M, Shahid M, Pan W. Low radiative heat transfer realized by $8YSZ/LaAl_{11}O_{18}$ composites for high-temperature applications. J Mater Sci. 2022;57(40):18754–69. doi:10.1007/s10853-022-07840-2

37. Altay A, Gülgün MA. Microstructural Evolution of Calcium-Doped α-Alumina. J Am Ceram Soc. 2003;86(4):623–9. doi:10.1111/j.1151-2916.2003.tb03349.x

38. Sktani ZDI, Rejab NA, Rosli AFZ, Arab A, Ahmad ZA. Effects of La_2O_3 addition on microstructure development and physical properties of harder $ZTA-CeO_2$ composites with sustainable high fracture toughness. J Rare Earths. 2020; doi:10.1016/j.jre.2020.06.005

39. Cherkasova N, Kuzmin R, Veselov S, Antropova K, Ruktuev A, Ogneva T, Tyurin A, Kuchumova I, Khabirov R. Influence of strontium hexaaluminate percentage on the structure and properties of alumina-zirconia ceramics. Mater Chem Phys. 2022;288:126424. doi:10.1016/j.matchemphys.2022.126424

40. Huang X, Cui J, Guan K, Rao P. Influence of La_2O_3 addition on microstructure and mechanical properties of alumina-dispersed zirconia. J Aust Ceram Soc. 2021;57(5):1407–14. doi:10.1007/s41779-021-00615-z

41. Wu H, Liu W, Lin L, Huang Z, Wei S, Wu S, Sun Z, An D, Xie Z. The rising crack resistance curve behavior and mechanism of La_2O_3 doped zirconia toughened alumina composites prepared via vat photopolymerization based 3D printing. Mater Chem Phys. 2022;285:126090. doi:10.1016/j.matchemphys.2022.126090